THE JOURNAL OF BIOLOGICAL CHEMISTRY VOL. 288, NO. 23, pp. 16629–16644, June 7, 2013

The *in Vivo* TRPV6 Protein Starts at a Non-AUG Triplet, Decoded as Methionine, Upstream of Canonical Initiation at AUG*[S]

Received for publication, March 18, 2013, and in revised form, April 19, 2013 Published, JBC Papers in Press, April 23, 2013, DOI 10.1074/jbc.M113.469726

Claudia Fecher-Trost[‡1,2], Ulrich Wissenbach[‡1,2], Andreas Beck[‡], Pascal Schalkowsky[‡], Christof Stoerger[‡], Janka Doerr[‡], Anna Dembek[‡], Martin Simon-Thomas[‡], Armin Weber[‡], Peter Wollenberg[‡], Thomas Ruppert[§], Ralf Middendorff[¶], Hans H. Maurer[‡], and Veit Flockerzi[‡2]

From the [‡]Institut für Experimentelle und Klinische Pharmakologie und Toxikologie, Universität des Saarlandes, 66421 Homburg, Germany, [§]Zentrum für Molekulare Biologie der Universität Heidelberg, Im Neuenheimer Feld 282, 69120 Heidelberg, Germany, and the [¶]Institut für Anatomie und Zellbiologie, Justus Liebig Universität Gießen, Aulweg 123, 35385 Giessen, Germany

Background: The TRPV6 amino acid sequence is predicted from its cDNA.
Results: The TRPV6 protein purified from human tissues has an extended N terminus not present in the predicted protein.
Conclusion: Full-length TRPV6 is trafficked to the plasma membrane, and its translation efficiency tightly controls TRPV6-mediated Ca^{2+} entry.
Significance: This study provides mechanistic insights into the function of the full-length TRPV6.

TRPV6 channels function as epithelial Ca^{2+} entry pathways in the epididymis, prostate, and placenta. However, the identity of the endogenous TRPV6 protein relies on predicted gene coding regions and is only known to a certain level of approximation. We show that *in vivo* the TRPV6 protein has an extended N terminus. Translation initiates at a non-AUG codon, at ACG, which is decoded by methionine and which is upstream of the annotated AUG, which is not used for initiation. The *in vitro* properties of channels formed by the extended full-length TRPV6 proteins and the so-far annotated and smaller TRPV6 are similar, but the extended N terminus increases trafficking to the plasma membrane and represents an additional scaffold for channel assembly. The increased translation of the smaller TRPV6 cDNA version may overestimate the *in vivo* situation where translation efficiency may represent an additional mechanism to tightly control the TRPV6-mediated Ca^{2+} entry to prevent deleterious Ca^{2+} overload.

During the last 15 years TRP[3] channel proteins have been extensively characterized, but direct experimental evidence of TRP protein sequences present *in vivo* are not available. This limitation not only refers to TRP channel genes but to most protein-coding genes in human and many other organisms. So far, 98% of the protein sequences provided by the UniProt resource come from translations of submitted coding sequences by gene prediction programs, and only about 5% of the protein entries contain sequence data obtained by direct protein sequencing, by Edman degradation, or MS/MS experiments (UniProt). Although new developments in protein analytical methods including mass spectrometry-based targeted proteomics will improve this situation in the future, current approaches primarily rely on antibodies to pull out the protein of interest from complex biological samples. However, adequate antibodies for most TRP proteins, which are low-abundant proteins, are not generally available (1).

TRPV6 (TRP channel, vanilloid type 6) cDNAs were cloned (2–4), and transcripts were identified in the placental trophoblasts, pancreatic acinar cells, salivary gland cells, and cancerous prostate (4). After overexpression of its complementary DNA (cDNA) in the human embryonic kidney (HEK293) cell line, TRPV6 forms plasmalemmal ion channels leading to selective Ca^{2+} influx as long as the intracellular Ca^{2+} concentration is kept low by BAPTA or related chelators. Only recently, TRPV6 has been shown to be critical for Ca^{2+} absorption through the epididymal and prostate epithelium (5, 6). Both the replacement of a single amino acid residue within the TRPV6 channel pore, D542A, in mice or deletion of the wild-type *TRPV6* gene in mice by gene targeting cause severe defects in male fertility, motility, and viability of sperm and a significant increase in the epididymal and prostatic luminal Ca^{2+} concentrations. Based on these data, TRPV6 is assumed to be an epithelial Ca^{2+} uptake channel. In contrast to these functional properties, little is known about the endogenous TRPV6 proteins mainly because of their low abundance and the lack of appropriate antibodies.

We have now generated several antibodies for TRPV6 (7, 8) and used them for an antibody-based affinity purification scheme, which allowed TRPV6 proteins to be enriched from human placenta and the human breast cancer cell line T47D, a

* This work was supported by the Deutsche Forschungsgemeinschaft (to C. F.-T., A. B., P. S., and V. F.), Forschungsausschuss der Medizinischen Fakultät "HOMFOR," and Forschungsausschuss der Universität des Saarlandes (to U. W., H. H. M., and V. F.).
[S] This article contains supplemental Table 1 and Fig. 1.
[1] Both authors contributed equally.
[2] To whom correspondence may be addressed: Institut für Experimentelle und Klinische Pharmakologie und Toxikologie, Universität des Saarlandes, Geb. 46, 66421 Homburg, Germany. E-mail: claudia.fecher-trost@uks.eu, ulrich.wissenbach@uks.eu, or veit.flockerzi@uks.eu.
[3] The abbreviations used are: TRP, transient receptor potential; Ab, antibody; Bis-Tris, 2-[bis(2-hydroxyethyl)amino]-2-(hydroxymethyl)propane-1,3-diol; V_h, holding potential; aa, amino acid; nt, nucleotide(s); A.U., absorbance units.

tissue (4) and a cell line (9) that have been shown to contain decent amounts of TRPV6 transcripts. Using site-specific antibodies, site-directed mutagenesis, and mass spectrometry, we show that translation initiation occurs at the ACG codon within the annotated 5′-UTR of *TRPV6* in the RefSeqGene (www.ncbi.nlm.nih.gov), which is decoded by methionine. In contrast to *KCNK2* and *KCNK10*, the genes encoding K2p2.1 (or TREK-1) and K2p10.1 (or TREK-2), which generate "full-length" and N-terminal truncated potassium channel proteins via translation initiation at alternative canonical AUG codons (10, 11), the human and mouse *TRPV6* genes *in vivo* generate exclusively the full-length TRPV6 proteins. A larger fraction of the full-length protein is associated with the cell surface where the extended N terminus represents an additional scaffold for yet to be identified interacting proteins and regulatory molecules.

EXPERIMENTAL PROCEDURES

Antibody-based Affinity Purification—Use of human tissue was approved by the local state's ethical committee (Ethik-Kommission der Ärztekammer des Saarlandes, Saarbrücken, Germany). 100 μg of affinity-purified antibodies were covalently coupled to magnetic M-280 tosyl-activated beads (Invitrogen) in the presence of phosphate buffer (0.1 M NaH_2PO_4/Na_2HPO_4, pH 7.4) and ammonium sulfate buffer (3 M $(NH_4)_2SO_4$) for 12–16 h at 37 °C. Blocking was performed in the presence of PBS, pH 7.4, with 0.5% (w/v) BSA for 1 h at 37 °C. The beads were washed 3 times with PBS, pH 7.4, with 0.1% (w/v) BSA and 0.05% NaN_3 and stored in the same buffer at 4 °C until use. Microsomal membrane protein fractions (500 mg) prepared from human placenta (in average starting with 100 *g* tissue) according to Stumpf *et al.* (8) were resuspended in 75 ml of radioimmune precipitation assay buffer (150 mM NaCl, 50 mM Tris HCl, pH 8.0, 5 mM EDTA, 1% Nonidet P40, 0.1% SDS, 0.5% sodium deoxycholate, pH 7.4), homogenized with a glass Teflon potter, and incubated by shaking for 45 min at 4 °C. After centrifugation at 100,000 × *g* at 4 °C for 45 min, the supernatant containing the solubilized proteins was incubated with the antibodies coupled to magnetic beads for 2–16 h at 4 °C. The beads were collected with a magnetic rack and washed with 1 ml of radioimmune precipitation assay buffer six times. For Western blot and for Coomassie-stained gels (mass spectrometry) the proteins were eluted with 40–60 μl of denaturing sample buffer (final concentration: 60 mM Tris HCl, pH 6.8, 4% SDS, 10% glycerol including 0.72 M β-mercaptoethanol) at 60 °C for 20 min.

Antibodies—The following in-house-generated anti-TRPV6 antibodies were used: polyclonal antibody (Ab) 429 and monoclonal Abs 20C6 and 26B3, both for the C terminus of TRPV6 (6, 7), and the polyclonal Abs 1271, 1272, and 1286, directed against the elongated N terminus of human and mouse TRPV6. All antibodies were affinity-purified before use. Antibodies for GFP were from Roche Applied Science (mixture of two mouse monoclonal Abs), for β-actin from Abcam (rabbit polyclonal Ab).

Cloning of TRPV6 Expression Constructs—The cDNA of human TRPV6 (NCBI reference sequence NM_018646.3) was subcloned into the bicistronic expression vector pcAGGS-IRES-GFP as described earlier (4). The vector allows simultaneous expression of the TRPV6 and the GFP cDNAs. The predicted 5′-UTR was completely removed, and the consensus sequence for initiation of translation in vertebrates GCCGCCACC (12) was introduced immediately upstream of the first AUG codon of the TRPV6 cDNA (see Fig. 1*D*, small TRPV6 variant or TRPV6-S). This Kozak sequence was then replaced within this expression construct by the complete predicted 5′-UTR of the human TRPV6 (nucleotides 1–229 of NM_018646.3) obtained from a TRPV6 cDNA clone isolated from a human placenta library (4) to obtain the very long TRPV6 variant (*TRPV6-XL*, see Fig. 1*D*). Using a similar strategy a Kozak sequence was introduced upstream of the ACG codon (position −120 to −118 of the predicted 5′-UTR) resulting in the long TRPV6 variant (*TRPV6-L*, see Fig. 1*D*). The TRPV6-L and TRPV6-XL constructs were used to insert mutations as shown in Fig. 3. For *in vitro* transcription/translation experiments the cDNAs encoding methionine (Met^{+1} of the annotated human TRPV6 sequence) to glutamate (Glu^{46}) and the corresponding 5′ nucleotides of TRPV6-S, TRPV6-L, and TRPV6-XL were fused to the GFP cDNA and subcloned into pcDNA3 (see Fig. 3, *D* and *F*). The corresponding mouse TRPV6 cDNAs (see Fig. 4*F*) were constructed accordingly based on the NCBI reference sequence NM_022413.4 with the 5′ region upstream of the first AUG amplified from genomic DNA. For experiments on protein stability and confocal microscopy, the D542A pore mutation was introduced in the hTRPV6-S and hTRPV6-XL variants by *in vitro* mutagenesis. For glutathione *S*-transferase (GST) pulldown assay a fragment of the TRPV6 cDNA (nucleotides −120 to +78) was fused to the GST cDNA and cloned in pGEX2T (GE Healthcare). All cloning steps that required PCR amplification were done with the Phusion polymerase (5), and all cDNA constructs were sequenced before use.

Gel Electrophoresis of Proteins and Mass Spectrometry—Proteins eluted from antibody-loaded magnetic beads were separated on NuPAGE® 4–12% gradient gels, fixed in the presence of 40% ethanol and 10% acetic acid, and visualized with colloidal Coomassie stain (20% (v/v) methanol, 10% (v/v) phosphoric acid, 10% (w/v) ammonium sulfate, 0.12% (w/v) Coomassie G-250) (13). Gel pieces were cut out and alternately washed twice with solution A (50 mM NH_4HCO_3) and solution B (50 mM NH_4HCO_3 and 50% (v/v) acetonitrile). Reduction of disulfide bridges was obtained by incubation at 56 °C for 30 min in 50 mM NH_4HCO_3 and 10 mM dithiothreitol followed by carbamidomethylation at 21 °C in darkness for 30 min in the presence of a solution containing 50 mM NH_4HCO_3 and 5 mM iodoacetamide. Gel pieces were washed twice alternating with solution A and B and then dried in a vacuum centrifuge. For in-gel digestion the gel pieces were incubated in the presence of 5–15 μl of porcine trypsin (10 ng/μl, Promega) at 37 °C overnight. Resulting peptides were extracted twice by shaking the gel pieces in aqueous extraction buffer (2.5% formic acid, 50% acetonitrile). Extracted peptides were concentrated in a vacuum centrifuge and resuspended in 0.1% formic acid.

Nano-LC-HR-MS/MS—An aliquot (1–10 μl) of the tryptic peptide extracts for each antibody purification was analyzed by online nanoflow LC-HR-MS/MS (Ultimate 3000 RSLC nano

system equipped with an Ultimate3000 RS autosampler coupled to an LTQ Orbitrap Velos Pro, all ThermoFisher Scientific, Dreieich, Germany). Peptides were trapped on a C18 trap column (75 μm × 2 cm, Acclaim PepMap100C18, 3 μm, Dionex) and separated on a reversed phase column (nano viper Acclaim PepMap capillary column, C18; 2 μm; 75 μm × 15 cm or 75 μm × 25 cm, Dionex) at a flow rate of 300 nl/min with buffer A (water and 0.1% formic acid) and B (90% acetonitrile and 0.1% formic acid) using gradient 1 (4 to 55% buffer B in 30 min; 55 to 90% B in 6 min), and gradient 2 (4 to 55% buffer B in 55 min; 55 to 90% B in 5 min). The effluent of the chromatography was directly sprayed into the mass spectrometer through a coated silica electrospray emitter (PicoTipEmitter, 30 μm, New Objective, Woburn, MA) and ionized at 2.2 kV. MS spectra were acquired in a data-dependent mode (automatic switch between full scan MS and MS/MS). For the collision-induced dissociation MS/MS top10 method (gradients 1 and 2), full scan MS spectra (m/z 300–1700) were acquired in the Orbitrap analyzer using a target value of 10^6. The 10 most intense peptide ions with charge states >2 were fragmented in the high pressure linear ion trap by low energy collision-induced dissociation with a normalized collision energy of 35%. For the high energy collision dissociation top3 method (gradient 1), full scan MS spectra (m/z 300–1700) were recorded in the Orbitrap analyzer with resolution of $r = 60{,}000$. The 3 most intense peptide ions with charge states >2 were sequentially isolated and fragmented in the high energy collision dissociation collision cell with normalized collision energy of 30%. The resulting fragments were detected in the Orbitrap system with resolution $r =$ 7500. Data for one protein purification from placenta with Ab 20C6 were acquired on an Eksigent-ESI-LTQ Orbitrap XL system in a similar way.

Raw LC-MS Data Analysis—The fragmented peptides were identified by using MASCOT algorithm and ThermoFisher Scientific Proteome Discoverer 1.3 software. Peptides were matched to tandem mass spectra by Mascot Version 2.4.0 (Matrix Science, London, UK) by searching an in-house modified SwissProt database (version2012_03, April 14th, 2012, number of protein sequences 535.251). MS^2 spectra were matched with a mass tolerance of 7 ppm for precursor masses and 0.5 Da for fragment ions. We used semi-tryptic digest, which considers that one of the cleavage sites is tryptic, but the other site may be at any residue and allowed for up to two missed cleavage sites. Cysteine carbamidomethylation was set as a fixed modification, and deamidation of asparagine and glutamine, acetylation of lysine, and oxidation of methionine were set as variable modifications.

Confocal Microscopy—For confocal microscopy HEK293 cells were co-transfected with the TRPV6-S or the TRPV6-XL cDNAs (with or without the pore mutation, D542A) fused to the eGFP cDNA and the pCherryPicker cDNA (Clontech), a vector that constitutively expresses the cDNA of the red fluorescent protein mCherry (14) fused to the cDNA of the transferrin receptor membrane-anchor domain (15); the fusion protein was used as a plasma membrane marker. The cDNA of tmem 16a cloned from human placenta and fused to the GFP cDNA was expressed as independent control. Cells were plated on lysine-coated coverslips. The distribution of TRPV6-XL and TRPV6-S perpendicular to the cell membrane was studied in fluorescence images using dedicated software, which was written in Delphi 2010 (Embarcadero). This software was employed for the transformation of images as well as for the accumulation of the relevant data. Appropriate membrane segments were identified (see Fig. 6*Ab*), and the fluorescence image rotated so that the membrane segment under investigation was angled almost vertically. In the next step, the red fluorescence defining the cell membrane was traced manually, and the resulting, more or less jagged, manual track was smoothed using a moving average filter. A region of interest was defined to the left and right of the smoothed track. The membrane was linearized for further processing by cross-correlating the red fluorescence inside the region of interest of individual scan lines with the center scan line of the membrane segment (see Fig. 6*A*, *c* and *d*). The scan line in this context means the row of pixels belonging to the same y-value of the rectangular cutout of the rotated image of the membrane segment under investigation. After linearization of the membrane, fluorescence intensities of the green and red fluorescence image were summed up column-wise over all scan lines of a membrane segment, yielding a cumulative fluorescence signal for each membrane sample. Background subtraction was done semi-automatically as well as was the localization of the red peak value, with manual correction if necessary (see Fig. 6*Ae*). The resulting curves were flipped if required, so that the extracellular space was located to the right of the resulting fluorescence intensity distribution for each membrane segment. Due to different expressions of the fluorescent probes in different cells and the different length of the membrane samples, normalization of the obtained sums was required. This was achieved using a two-step approach. In the first step, the mean and S.D. of the summed fluorescence intensities in each column of a membrane segment were calculated, and the intensities were z-transformed with the obtained mean and S.D., which resulted in a mean total fluorescence of zero and a S.D. of 1 for each membrane sample. This was done for the red as well as for the green signal. In a second step, the resulting transformed sums were retransformed so as to minimize the sum of squares of differences between all membrane probes of a given protein (TRPV6-S, TRPV6-XL, CherryPicker, and tmem 16a). The rationale behind this two-step approach was to render the curves of the different proteins comparable (step 1) and to minimize the variation between individual samples of a single protein (step 2). Before the second transformation, all samples were shifted along the x axis until their red peaks were aligned, and a band of 14 pixels to either side of the red peak was used for further analysis. It should be emphasized here that the absolute intensities of the signals are irrelevant, as only the shape of the fluorescence intensity distribution perpendicular to the membrane was to be considered.

After the two normalization steps, weighted means and 95% confidence intervals were calculated for the normalized intensities of each protein using the number of scan lines in each membrane sample as a weight. The resulting curves are shown in Fig. 6*Aa*. As can be seen, CherryPicker and tmem 16a both peak at the cell membrane, whereas TRPV6-XL and TRPV6-S appear not to be strongly associated with the membrane. As judged from the overlap of the 95% confidence intervals of their

fluorescence distributions, a gross difference in association with the cell membrane may be excluded.

Data Analysis—Initial patch clamp and Ca^{2+} imaging analysis was performed with FitMaster (HEKA) and TILLvisION (TILL Photonics), respectively. IGOR Pro (Wave Metrics, Lake Oswego, OR) was used for further analysis and for preparing the figures. Where applicable the data were averaged and given as the means ± S.E. for a number (n) of cells or x-averaged experiments including n measured cells (x/n). In Western blots, proteins were detected with horseradish peroxidase-coupled secondary antibodies and the Western Lightning Chemiluminescence Reagent Plus (PerkinElmer Life Sciences). Original scans were saved as TIFF files from LAS 3000 (Fujifilm), which were further processed in Adobe Photoshop. Stain intensities were analyzed by the Aida Image Analyzer software. Images were cropped, resized proportionally, and brought to the resolution required for publication.

Surface Biotinylation, Western Blot, and Image Processing—One flask (75 cm^2) with confluent COS cells or HEK293 cells, respectively, transfected and cultured for 48 h, was placed on ice, washed twice with ice-cold phosphate-buffered saline (137 mM NaCl, 2.7 mM KCl, 10 mM Na_2HPO_4, 2 mM KH_2PO_4) containing 1 mM $MgCl_2$ and 0.5 mM $CaCl_2$ (PBSB), and incubated in the presence of NHS-LC-biotin freshly diluted in PBSB at 0.5 mg/ml for 30 min at 4 °C. The reaction was stopped by washing twice with PBSB containing 0.1% (w/v) bovine serum albumin and once with PBS, pH 7.4. Cells were harvested from the flasks by shaking in PBS supplemented with 2 mM EDTA. The harvested cells were centrifuged at 1000 × g at 4 °C for 5 min and resuspended in ice-cold lysis buffer (PBS containing 1% Triton X-100, 1 mM EDTA, and a mixture of protease inhibitors). Cell lysates were rotated at 4 °C for 30 min to solubilize proteins; after centrifugation at 1000 × g and 4 °C for 5 min, protein was determined using BCA (Pierce), and the protein solution (1–2 mg) was added to 100 μl of avidin-agarose beads preequilibrated in lysis buffer and incubated at 4 °C for 2 h. The biotin-avidin-agarose complexes were washed 4 times with lysis buffer supplemented with 0.25 M NaCl. Biotinylated proteins were eluted in 100 μl of 2-times denaturing electrophoresis sample buffer and incubated at 60 °C for 30 min before SDS-polyacrylamide gel electrophoresis (SDS-PAGE) on 4–12% Bis-Tris gels (NuPAGE®-Novex, Invitrogen) in a MOPS buffer system (50 mM MOPS, 50 mM Tris, 0.1% SDS, 1 mM EDTA, pH 7.7). Input corresponds to protein samples taken before adding avidin-agarose beads. The proteins were electrophoretically separated, blotted, and probed with Ab 429 and Ab 1271, respectively. The endoplasmic reticulum protein calnexin was probed for biotinylation as a control.

Protein Stability Assay—HEK 293 cells were transfected with the cDNA of the constructs TRPV6-S-D542A or TRPV6-XL-D542A in pcAGGS-GFP vector. 24 h after transfection the medium was changed, and 50 μg/ml cycloheximide in dimethyl sulfoxide (DMSO) or DMSO alone (time 0) was added to the cells. After various time points (0, 0.5, 3, 5, 7, 9, 24 h) cells were harvested and lysed in denaturing sample buffer and incubated at 60 °C for 20 min. 1/15 of the lysate was resolved under reducing conditions on NuPAGE® 4–12% gradient gels in the MOPS buffer system, and the proteins were transferred onto nitrocellulose membranes. The membranes were probed with antibodies against TRPV6 C terminus (26B3) and β-actin (Abcam) as a loading control.

Deglycosylation—The TRPV6 proteins enriched from human placenta and retained by the magnetic antibody-loaded magnetic beads were incubated in the presence of 2 μl of glycoprotein denaturing buffer (New England Biolabs) in a total volume of 20 μl for 20 min at 60 °C. The mixture was supplemented with 4 μl of 0.5 M sodium phosphate, pH 7.5, 4 μl of Nonidet P40, and 8 μl of H_2O. One-half of the reaction mixture was supplemented with 2 μl of *N*-glycosidase F (PNGase, New England Biolabs) or with 2 μl H_2O (PNGase negative control) and incubated for 1 h at 37 °C. Deglycosylation was stopped by adding 2-times concentrated denaturing sample buffer followed by incubation at 60 °C for 20 min.

In Vitro Translation—*In vitro* translation of the 3′-truncated TRPV6-S, TRPV6-L, and TRPV6-XL cDNAs fused to the GFP cDNA and subcloned into pcDNA3 under the control of the T7 promotor was performed with the coupled transcription/translation system TNT7 (Promega) in the presence of 25 μl of rabbit reticulocyte lysate, 1 μg of plasmid, and 100 μCi [^{35}S]methionine for 90 min at 30 °C. The reaction was stopped by adding denaturing sample buffer followed by incubation at 60 °C for 20 min. The *in vitro* translated products were applied to SDS-PAGE and processed as described.

Immunofluorescence and Immunohistochemistry—Human placenta tissue was frozen in liquid nitrogen and embedded in optimal cutting temperature (OCT) compound (Tissue Tek, Sakura, Zoeterwoude, The Netherlands). For immunofluorescence labeling, 10-μm-thick frozen sections were prepared, air-dried, and fixed with acetone for 10 min. After air-drying, washing in PBS, and blocking of unspecific protein binding sites by 2% normal goat serum (Sigma) in PBS for 30 min, sections were incubated in antibody buffer (0.2% bovine serum albumin, 0.1% NaN_3 in PBS) at 4 °C overnight with the monoclonal mouse anti-TRPV6 antibody 20C6 (1:20), directed against the C terminus of human (and mouse) TRPV6, as well as with the rabbit polyclonal antibodies 1271 and 1272 (1:200 each), detecting only the XL-version of human TRPV6. Then sections were washed in PBS and incubated with Alexa Fluor 488 goat anti-mouse IgG (1:500, Molecular Probes, Eugene, OR), CY3-goat anti mouse (1:500, Dianova), Alexa Fluor 488 goat anti-rabbit IgG (1:500, Molecular Probes), and CY3-goat anti rabbit IgG (1:500, Dianova), each in PBS for 1 h at room temperature. Finally, sections were washed in PBS, post-fixed in 4% paraformaldehyde in PBS, washed again in PBS, and mounted in buffered glycerol.

Cell Culture and Transfection—HEK293 cells were grown in 3-cm-diameter culture dishes with and without polylysine-coated glass coverslips (diameter 2.5 cm) until 80% confluence and then transiently transfected with 4 μg of the respective cDNA constructs described above in 5 ml of the PolyFect® reagent (Qiagen, Hilden, Germany). For Fura-2 measurements, cells transfected with the pcAGGS-IRES-GFP vector were used as controls. Coverslips with transfected cells were used for Ca^{2+} imaging experiments 24–48 h after transfection. Dishes without coverslips were trypsinized, and transfected cells were

plated on 1-cm polylysine-coated glass coverslips for patch clamp experiments, also performed 24–48 h after transfection.

Electrophysiological Recordings and Solutions—Membrane currents were recorded in the tight seal whole cell patch clamp configuration using an EPC-9 amplifier (HEKA Electronics, Lambrecht, Germany). Patch pipettes were pulled from glass capillaries GB150T-8P (Science Products, Hofheim, Germany) at a P-1000 micropipette puller (Sutter Instruments, Novato, CA) and had resistances between 2 and 4 megaohms when filled with internal solution (140 mM cesium glutamate, 8 mM NaCl, 1 mM $MgCl_2$, 10 mM HEPES, 10 mM cesium-BAPTA, pH adjusted to 7.2 with CsOH). Standard external solution contained 140 mM NaCl, 10 mM CsCl, 2 mM $MgCl_2$, 10 mM $CaCl_2$, 10 mM HEPES, 10 mM glucose, pH adjusted to 7.2 with NaOH. Where indicated, divalent-free saline, based on standard external solution without Ca^{2+} and Mg^{2+} but with 10 mM EGTA, was pressure-applied directly onto the patch-clamped cell by a patch pipette with a slightly broken tip. Osmolarity of all solutions ranged between 285 and 305 mosM. Voltage ramps of 50-ms duration spanning a voltage range from −100 to +100 mV were applied at 0.5 Hz from a holding potential (V_h) of 0 mV over a period of up to 300 s using the PatchMaster software (HEKA). All voltages were corrected for a 10-mV liquid junction potential. Currents were filtered at 2.9 kHz and digitized at 100-μs intervals. Capacitive currents and series resistances were determined and corrected before each voltage ramp using the automatic capacitance compensation of the EPC-9. Basic currents at break-in were subtracted, and inward and outward currents were extracted from each individual ramp current recording by measuring the current amplitudes at −80 and +80 mV, respectively, and plotted *versus* time. Representative current-voltage relationships (IVs) were extracted at the indicated time points. In some experiments 400-ms and 10-s voltage steps to −100 mV were applied, and currents were measured at higher temporal resolution of 1 kHz. All currents were normalized to the cell size (picoamperes/picofarads).

Ca^{2+} Imaging—Intracellular live cell Ca^{2+} imaging experiments were performed using a Polychrome V and CCD camera (TILL Imago)-based imaging system from TILL Photonics (Martinsried, Germany) with a Zeiss Axiovert S100 fluorescence microscope equipped with a Zeiss Fluar 20×/0.75 objective. Data acquisition was accomplished with the imaging software TILLvisION (TILL Photonics). Before the experiments, cells were incubated in media supplemented with 4 μM Ca^{2+}-sensitive fluorescent dye Fura-2-AM for 30 min in the dark at room temperature and washed 4 times with nominally Ca^{2+}-free external solution (140 mM NaCl, 5 mM KCl, 1 mM $MgCl_2$, 10 mM HEPES, 10 mM glucose, pH adjusted to 7.2 with NaOH) to remove excess Fura-2-AM. The Fura-2-loaded cells, growing on 2.5-cm glass coverslips, were transferred to a bath chamber containing nominally Ca^{2+}-free solution, and Fura-2 fluorescence emission was monitored at >510 nm after excitation at 340 and 380 nm for 30 ms each at a rate of 1 Hz for 600 s. Cells were marked, and the ratio of the background-corrected Fura-2 fluorescence at 340 and 380 nm (F_{340}/F_{380}) were plotted *versus* time. After reaching a stable F_{340}/F_{380} base line, 2.5 mM $CaCl_2$ was added to the bath solution, and cytosolic Ca^{2+} signals were measured.

RESULTS

An N-terminal-extended TRPV6 Is Expressed in Placenta—To enrich the TRPV6 protein, we solubilized proteins from microsomal membrane fractions obtained from human placenta and applied an affinity purification using the Ab 20C6, which was directed to the C terminus of the TRPV6 protein (Fig. 1*A*). Eluted proteins were run on SDS-PAGE, blotted, and the TRPV6 protein was detected by the Ab 429. The placenta TRPV6 protein was detected as a broad band at ~80 kDa (Fig. 1*A*), which may represent the monomer, a band of slightly lower electrophoretic mobility that represents glycosylated versions (see also Fig. 5*E*), and a band representing higher molecular weight multimers. As a control, the human TRPV6 protein obtained after expression of its annotated protein coding cDNA in COS-7 (COS) cells was applied to the same gel and immunoblot. We noted that the major monomer, the glycosylated version, and the multimer of the TRPV6 expressed in COS cells migrated slightly faster compared with the placenta protein, indicating that a TRPV6 variant of higher molecular weight is present in the human tissue. TRPV6 variants have not been published so far with the exception of an allelic variant present in humans that exhibits three amino acid exchanges (4). There is also no evidence for TRPV6 splice variants,[4] which could explain the slower electrophoretic mobility of the TRPV6 protein enriched from human tissue.

Like most *TRP* genes, *TRPV6* orthologues are expressed in mammals, frogs, and fish. We used the sequence information from databases to translate the nucleotide sequences 5′ of the annotated initiation AUG codons (Fig. 1*B* and Table 1). The mammalian sequences upstream of the first AUG codon are conserved, but the one from rabbit contains an in-frame stop codon. In contrast, sequences from the other organisms contained several stop codons upstream of the annotated AUG and are not conserved. Sequence identity is highest among the 40 amino acids upstream of the first Met residue (position +1 in Fig. 1*B*). Therefore, it could be that translation starts at a non-AUG, although this appears to be a rare event in mammals (16–18). In these rare cases the codon for initiation differs by only one base from the canonical AUG codon (19). A codon meeting these requirements is the ACG at position −120 to −118 of the 5′-UTR, which is downstream of the stop codon of the rabbit 5′-UTR (Fig. 1*B*) and within the open reading frame of the predicted TRPV6 protein; it codes for threonine. Next we generated antibodies directed to the amino acid (aa) sequences translated from the nt −117 to −61 (Ab 1271, Fig. 1*C*) and repeated the Western blot of Fig. 1*A* using Ab 1271 (Fig. 1*C*). It recognizes the human placenta TRPV6 protein but not the TRPV6 protein in COS cells, indicating that a N-terminally extended TRPV6 protein exists in the human tissue.

Next, we cloned three TRPV6 cDNA constructs (Fig. 1*D*) into an expression vector: (i) TRPV6-small (TRPV6-S) containing the annotated protein-coding TRPV6 cDNA, which starts with the initiation AUG and is devoid of the putative 5′-UTR (20), (ii) TRPV6-large (TRPV6-L) containing the additional 120 nucleotides of the putative 5′-UTR upstream of the annotated

[4] U. Wissenbach, non-published data.

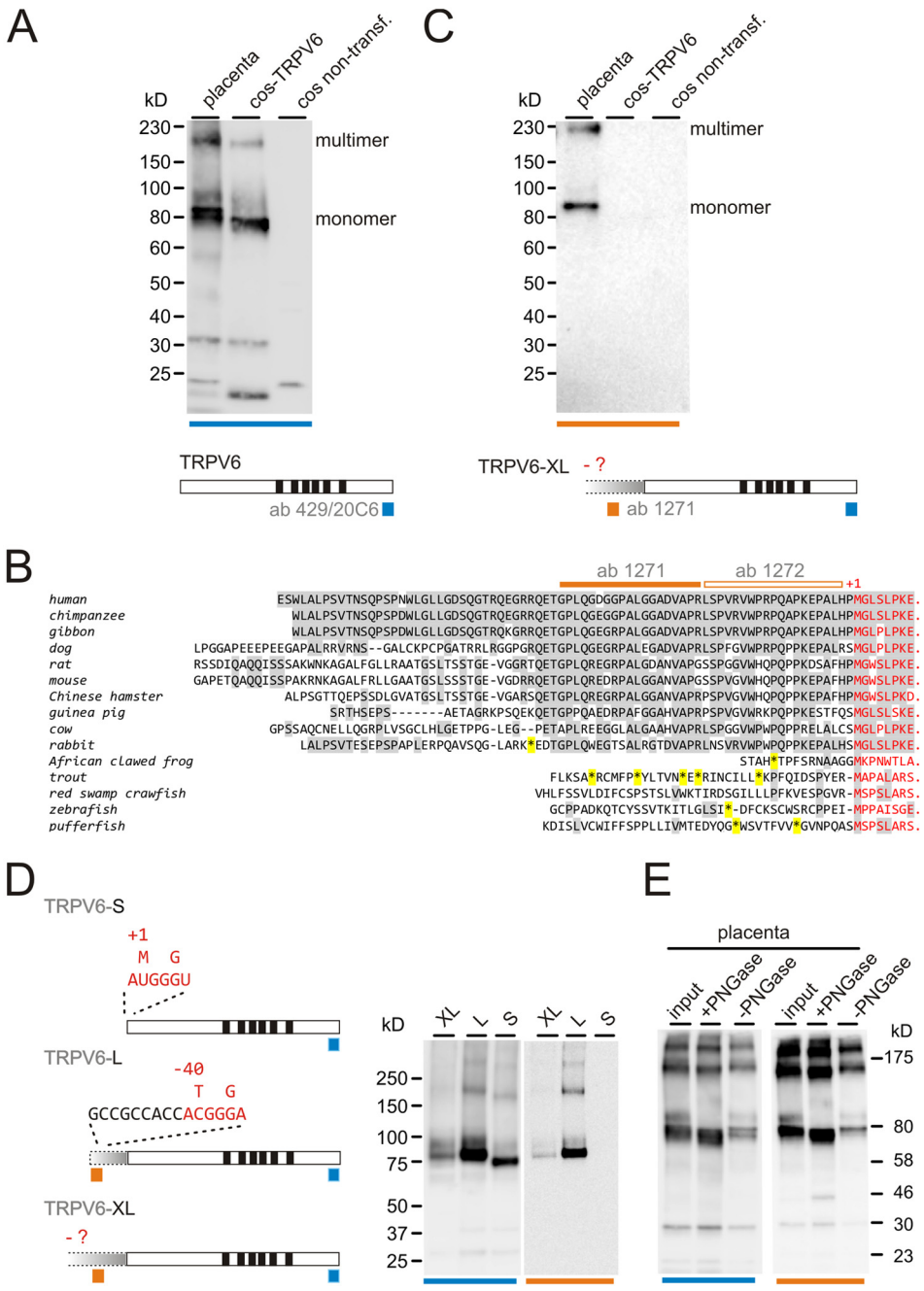

FIGURE 1. **Expression of the TRPV6 protein in human placenta.** *A*, an immunoblot is shown. The TRPV6 protein (~80 kDa) enriched from human placenta (*left lane*) by antibody-based affinity purification and after expression of the TRPV6 cDNA in COS cells (*middle lane*, 5 μl of lysate) was detected by Ab 429 (*blue square*). *Right lane*, lysates of non-transfected COS cells are shown. The *bar* indicates the aa sequence of the annotated TRPV6 protein with the six predicted transmembrane domains in *black* and the sequence recognized by Ab 20C6 and Ab 429 (*blue square*). *B*, shown is MUSCLE multiple sequence alignment of the translated 5′-UTR of TRPV6 as available for the organisms indicated (for accession numbers, see Table 1). Identical aa residues (compared with the human sequence) are *shaded*; annotated N termini with the first Met^{+1} are in *red*; *, stop codon in frame; −, gap; epitopes for Ab 1271 (*orange bar*) and Ab 1272 (*open orange bar*). *C*, the immunoblot is as in *A* but incubated with the Ab 1271 (*orange square*) directed against a translated sequence of the annotated 5′-UTR of human TRPV6 (GenBank™ accession number NM_018646.3). *D*, shown is expression of the TRPV6 cDNA constructs "small" (TRPV6-S, starting with the first AUG in frame encoding the first methionine, +1), "large" (TRPV6-L, forced to start with threonine, −40, by the 5′ inserted KOZAK sequence, indicated), and "very large" (TRPV6-XL, containing the complete 5′-UTR of the human TRPV6 gene) in COS cells and detected by Ab 20C6 (*blue*, *left panel*) and 1271 (*orange*, *right panel*). *E*, TRPV6-XL protein enriched by antibody-based affinity purification from human placenta is glycosylated. Affinity-purified TRPV6 (*lane 1*, *input*) and after 1 h of incubation at 37 °C in the presence (*lane 2*) and absence (*lane 3*) of *N*-glycosidase F (*PNGase*) are shown. Western blots and (*bottom*) region of TRPV6 recognized by antibody 20C6 (*blue*) and antibody 1271 (*orange*) shown are.

AUG starting with the ACG coding for Thr^{-40}, and (iii) TRPV6-very large (TRPV6-XL) containing the complete putative 5′-UTR (246 nucleotides) and expressed these cDNAs in COS cells. A consensus sequence for the initiation of translation in vertebrates (12) was inserted in front of the annotated initiation AUG in (i) and in front of the ACG codon (coding for the Thr at position −40). All three cDNAs were expressed, and the proteins were recognized by the antibody for their common

TABLE 1
Sources of the *TRPV6* 5′-UTR sequences used for alignments

Species	Common name	GenBank™ accession number
Homo sapiens	Human	NT_007914.15
Pan troglodytes	Chimpanzee	NC_006474.3
Nomascus leucogenys	Gibbon	NW_003501441.1
Canis lupus familiaris	Dog	NC_006598.3
Rattus norvegicus	Rat	NC_005103.3
Mus musculus	Mouse	NT_039353.8
Cricetulus griseus	Chinese hamster	NW_003614056.1
Cavia porcellus	Guinea pig	NT_176409.1
Bos bovis	Cow	NM_001206189.1
Oryctolagus cuniculus	Rabbit	NC_013675.1
Xenopus laevis	African clawed frog	EST BJ068625.1
Oncorhynchus mykiss	Trout	NM_001124455.1
Procambarus clarkii	Red swamp crawfish	AY452713.1
Danio rerio	Zebrafish,	NM_001001849
Takifugu rubripes	Pufferfish	NM_001032766.1

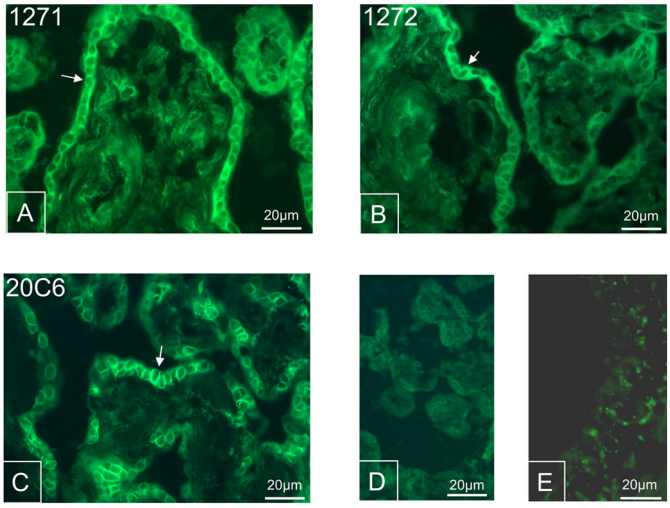

FIGURE 2. **Immunofluorescent staining of TRPV6 in human placenta tissue.** Staining of trophoblast cells (*arrows*) of placenta villus trees by abs 1271 (*A*), 1272 (*B*), and 20C6 (*C*) is shown. *D* and *E* are negative controls: photographs of placenta sections in the absence of primary antibody 20C6 (*D*) and 1271 and 1272 (*E*).

C terminus (Fig. 1*D*, *blue*). The TRPV6-L and the TRPV6-XL proteins migrated at a similar size, whereas TRPV6-S migrated faster. The antibody for the predicted N terminus recognized only the TRPV6-L and TRPV6-XL proteins (Fig. 1*D*, *orange*). These results indicate (i) the presence of the N-terminal-extended TRPV6 protein *in vivo* and (ii) exclusive formation of the extended protein variants rather than formation of both extended and small variants.

To test whether the antibodies against the extended N terminus of the TRPV6-L and XL versions (*Abs 1271* and *1272*, Fig. 1*B*) recognize the same structures of human placenta tissue as the antibody directed against the TRPV6 C terminus (20C6, Fig. 1*A*), immunofluorescence studies were performed. Trophoblast cells of villus stem and trees were stained by all three primary antibodies used (Fig. 2, *A*–*C*). Other structures did not show any specific immunostaining. Negative controls incubated with antibody buffer in the absence of primary antibodies were immuno-negative (Fig. 2, *D* and *E*).

Identification of the Initiation Triplet for Translation of TRPV6—The data so far demonstrate (i) that there is little if any difference in the electrophoretic mobility of the TRPV6-L and TRPV6-XL-variants (Fig. 1*D*) and (ii) that the elongated version contains at least a part of the sequence starting with $^{-40}$TGPL identified by Ab 1271 (Figs. 1*B* and 2*A*) (20). Accordingly, two of the non-canonical potential start codons, GUG (nt −72 to nt −70 for Val^{-24}; Fig. 3*A*, *red*) and CUG (nt −60 to −58, for Leu^{-20}, Fig. 3*A*, *red*) could be excluded, and the start codon must be identical with the one used within the TRPV6-L cDNA construct or in close proximity to this codon. The alignment of the 5′ nucleotide sequences of *TRPV6* from mammals revealed two additional non-AUG start codons, ACG (nt −120 to −118, for Thr^{-40}) and AGG (nt −132 to −130, for Arg^{-44}). First, the ACG codon was mutated (Fig. 3*B*), and the mutated TRPV6-L* cDNA constructs were subcloned into a bicistronic vector, which allows independent expression of the green fluorescent protein (GFP). Fig. 3*C* shows Western blots of lysates from COS cells expressing the constructs as indicated using antibodies for the common C terminus or the extended N terminus. Translation was dramatically reduced when the ACG codon was mutated to CCG (for Pro) or to ACU (for Thr); the latter mutation changed the codon but not the amino acid. In contrast, mutating the ACG to codons known to initiate translation like ATG (for Met) or CUG (for Leu) or mutating the GGA triplet (for Gly) 3′ of the ACG to ACA (for Thr) did not change protein expression compared with TRPV6-XL. To confirm these results by an independent approach, the cDNAs of the GFP and the cDNAs encoding the various TRPV6 N termini as indicated in Fig. 3*D* were fused. The fusion constructs were used for *in vitro* transcription/translation in a cell-free system, and the ^{35}S-labeled proteins was visualized by an x-ray film (Fig. 3*E*, *upper panel*) or by Western blot (Fig. 3*E*, *lower panel*). In this experiment, the same mutations as in Fig. 3, *B* and *C*, were introduced into the TRPV6-XL nucleotide sequence comprising the complete 246 nucleotides of the putative 5′-UTR and devoid of any additionally introduced sequence, which might facilitate transcription/translation. Because of the smaller size of the fusion proteins, the differences in molecular weight were more apparent, and the results obtained were very much identical to the data of Fig. 3*C*.

There is still the possibility that translation starts 5′ of the ACG, especially at the AGG (for Arg^{-44}, Fig. 3*A*). Therefore, additional mutations were introduced into the TRPV6-XL-GFP fusion construct (Fig. 3*F*). Either the AGG was removed completely, or the adjacent triplet AGA (for Arg^{-43}) was mutated to CGA, or both triplets were mutated to ACUCGU (for Thr^{-44}-Arg^{-43}), to UGGUGG (Trp^{-44}-Trp^{-43}), or replaced by two stop codons (TGATGA). Neither mutation had an effect on the *in vitro* translation product (Fig. 3*G*) compared with wild-type (TRPV6-XL), ruling out that a codon upstream of the Thr^{-40}-encoding ACG is used for translation.

Decoding of the ACG Initiation Codon as Methionine as Evidenced by Mass Spectrometry after Antibody-based Affinity Purification of TRPV6 Proteins from Human Placenta—TRPV6 proteins were enriched by the affinity purification scheme (Fig. 4, *A* and *B*) and analyzed by nano-LC-MS/MS (Fig. 4, *C*, *D*, and *E*). To identify peptide sequences from TRPV6, the searches were run against a custom database that was extended by adding the sequences of the predicted elongated N terminus (predicted aa −76 to −1) upstream of the annotated 725-aa TRPV6 human sequence (UniProtKB/Swiss-Prot Q9H1D0; Fig. 4*C*).

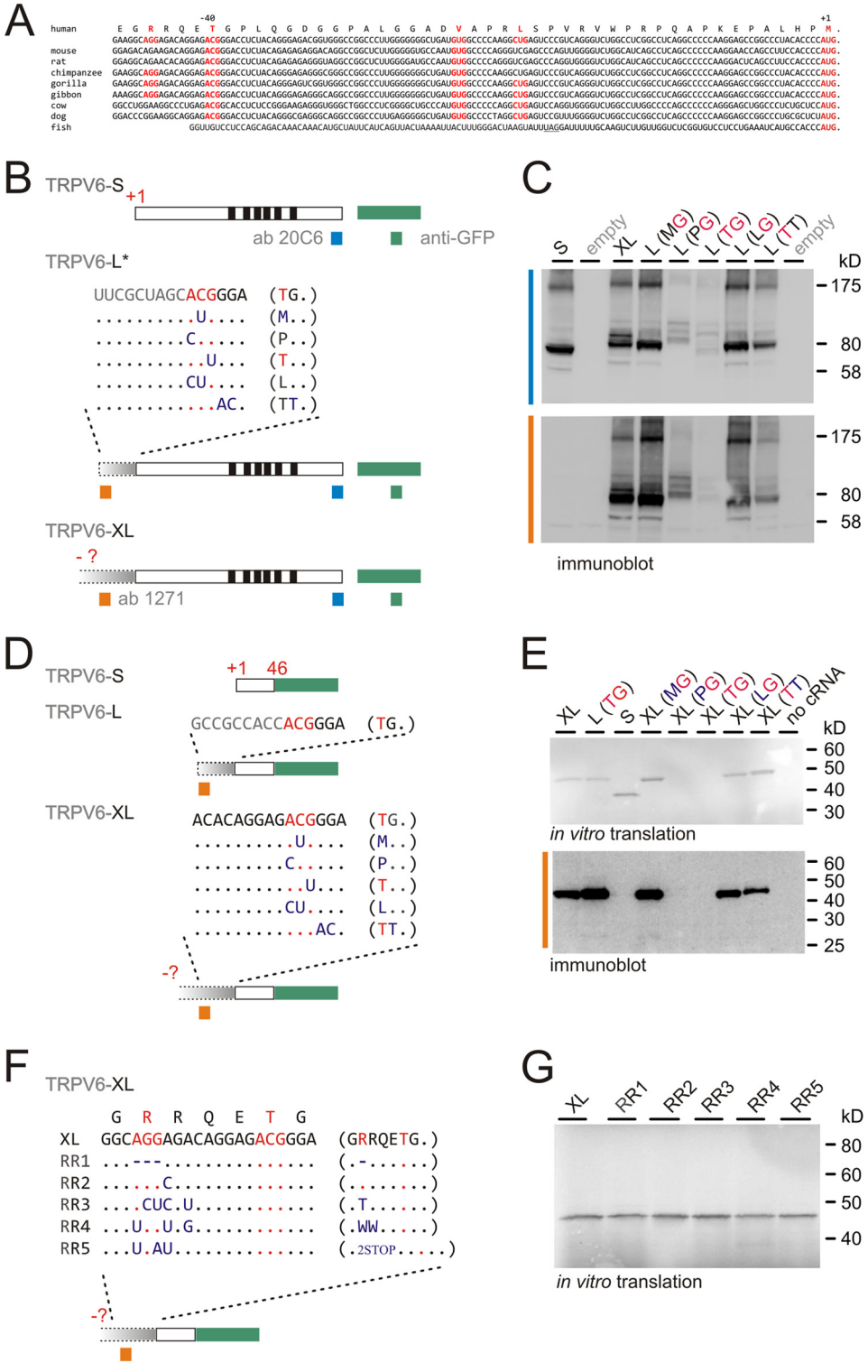

FIGURE 3. **Identification of translation initiation of the human TRPV6 protein.** *A*, shown is alignment of 5′-UTR TRPV6 sequences including the AUG triplet encoding the first methionine (*red*, +1) of the human protein. *Red*, putative initiation sites; *underlined*, STOP-codon in frame (GenBank™ accession numbers as in Table 1). *B* and *C*, The S, XL, and L hTRPV6 cDNAs were expressed in HEK293 cells; protein lysates of these cells were applied to SDS-PAGE electrophoresis, blotted, and incubated with Ab 20C6 (*C*, *blue*, *upper panel*) and Ab 1271 (*C*, *orange*, *lower panel*). The TRPV6-L* constructs contain an inserted nine-nucleotide 5′ sequence in front of the ACG codon (in *red*, for threonine (*T*)) very similar to the consensus sequence of the initiation of translation in vertebrates. Introduced mutations into the ACG codon (coding for threonine at position −40) and one mutation altering the 3′ codon (GGA) are indicated; the encoded aa are in *parentheses*. *D* and *E*, the cDNAs encoding the 46-aa N-terminal TRPV6 protein without (*S*) and with the complete 5′-UTR (*XL*) or the *L* sequence were fused with the GFP-cDNA. The *TRPV6-L* construct contains the 5′ inserted KOZAK sequence in front of the ACG codon (in *red*, for threonine (*T*). After *in vitro* transcription/translation, ^{35}S-labeled proteins were run on SDS-PAGE, which was then exposed to an x-ray film (*E*, *upper panel*) or blotted and incubated with Ab 1271 (*E*, *lower panel*). *F* and *G*, *in vitro* transcription/translation of the *TRPV6-XL*-GFP fusion construct carrying the indicated mutations in the potential upstream initiation codon AGG (*red*, for arginine (R)) and in the adjacent 3′-AGA codon with the resulting aa sequences in *parentheses*.

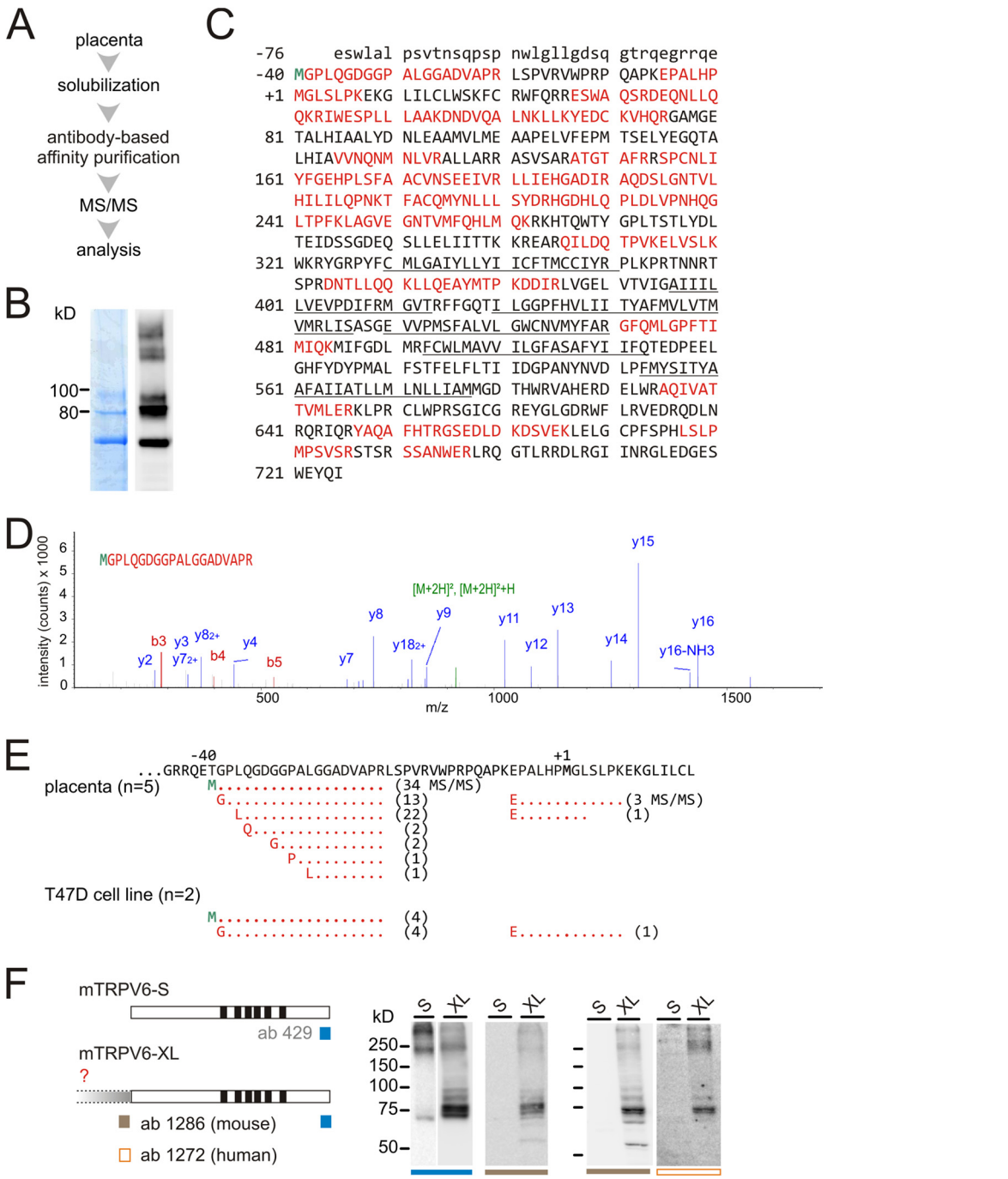

FIGURE 4. **Identification of the TRPV6 protein from human placenta.** *A*, workflow of TRPV6 affinity purification from placenta microsomal membranes and mass spectrometric analysis is shown. *B*, total eluates were separated on denaturing gels, stained with Coomassie (*left lane*), in-gel-trypsinized, and analyzed by nano-LC MS/MS spectrometry or blotted and incubated with antibody 429 recognizing the C terminus (*right lane*). *C*, shown is the predicted primary sequence of the human TRPV6 including the translated 5′-UTR (*capital letter*, experimental evidence; *lowercase*, no evidence) with the predicted Thr^{-40} replaced by the identified methionine (in *green*). Amino acids of all other peptides identified with nano-LC MS/MS are in *red* (sequence coverage 17.5–38.3; summary of all peptides are in supplemental Table 1), not identified aa are colored in *black*, and putative transmembrane segments are *underlined*. *D*, shown is the MS/MS fragmentation spectrum of the most upstream N-terminal TRPV6-derived peptide shown in *C*. *E*, *below the predicted amino acid sequence* (in *black*) the identified MS/MS sequences of the most upstream N-terminal TRPV6-derived peptides obtained from human placenta and from the T47D breast cancer cell line (*n*, number of independent purifications; number of MS/MS spectra in brackets) are shown. *F*, the translation start of murine TRPV6 is located upstream of the canonical AUG. Mouse TRPV6 cDNA expression constructs small (mTRPV6-S, starting with the first ATG in frame encoding the first methionine and devoid of the complete 5′-UTR) and very large (mTRPV6-XL, containing the complete 5′-UTR of the mouse TRPV6 gene) are shown. Western blot of protein lysates from transfected COS cells incubated in the presence of Ab 429 (*blue*, *left panel*), Ab 1272 (*orange*), and Ab 1286 (*brown*) is shown. The mTRPV6-XL is recognized by Ab 429, Ab 1286 (raised against the predicted mouse sequence), and Ab 1272 (raised against the predicted human sequence, which is 85% identical to the corresponding mouse sequence).

The TRPV6 protein was effectively purified by five independent purifications from human placenta and by two purifications from the human breast cancer T47D cell line by Ab 20C6 or 429 or Ab 1271 providing extensive coverage of its primary sequence (Fig. 4*C*) including the extended N terminus (supplemental Table 1). The most upstream localized peptides identi-

fied under this condition started at Gly^{-39}. It is important to note that only such peptides can be identified by an automated database search that are present in a database. The ACG codon for Thr^{-40} might be decoded by a Met rather than by a Thr, and the database was, therefore, changed again by replacing Thr^{-40} by Met. Now an additional peptide was identified: $^{-40}$MGPL . . . VAPR^{-21}. Fig. 4*D* shows the MS/MS fragmentation spectrum of this most upstream N-terminal TRPV6-derived peptide. It started with Met (in *green* in Fig. 4, *C–E*) at position −40. This peptide was also detected in various forms of the truncated N terminus; this could be caused by proteolytic processes during cell disruption and sample preparation. The number of fragment spectra for a specific peptide gives a good hint about the amount of this peptide (21). Using this spectral counting, the peptide including the N-terminal Met^{-40} is the most abundant peptide. Fig. 4*E* and supplemental Table 1 summarize all peptides obtained for the extended N terminus, and their frequencies were obtained under the latter conditions. In addition to consistently identifying Met^{-40} as the ACG-decoding residue, peptide sequences were obtained, which includes the annotated start Met (position +1, Fig. 4*E*) and part of the upstream primary sequence (Glu^{-6} to Lys^{+7}).

The Translation Start of Murine TRPV6 Like the One of Human TRPV6 Is Located Upstream of the Canonical AUG—Because of the high degree of identity of the annotated *TRPV6* 5′-UTR sequences from human and mouse (89.7%) (Figs. 1*B* and 3*A*), the mouse (m)TRPV6-S and mTRPV6-XL cDNA constructs were cloned (Fig. 4*F*) and expressed in COS cells. Western blots of protein lysates were probed by the antibody for the common C terminus and by antibodies for the predicted extended N terminus. The immunoblot (Fig. 4*F*) showed that the mTRPV6-XL was expressed at the expected increased size, indicating that also in mice the extended protein is responsible for *in vivo* TRPV6 activity.

Characterization of TRPV6-dependent Ca^{2+} Entry and Currents—So far characterization of TRPV6 channel activity primarily relies on the heterologous expression of the annotated cDNA encoding the protein sequence starting with the Met^{+1} (Figs. 1*C* and 4*C*). Here, we compared ion channel properties after expression of the various TRPV6 cDNAs in HEK 293 cells. Transfected cells were divided and checked for protein expression, changes of intracellular Ca^{2+} monitored by Fura-2-AM, and whole cell currents measured by patch clamp experiments. Transcription of the TRPV6-IRES-GFP cDNA (Fig. 5*A*) is controlled by the common vector promotor. The GFP translation efficiency was identical using the TRPV6-XL or TRPV6-S cDNAs (Fig. 5, *B*, *lower panel*, and *C*), and therefore, the intensity of the GFP immunostain was used as a control to estimate translation efficiencies of the two TRPV6 cDNAs. The XL version was expressed in 5.6-fold lower amounts than the S version (3 independent experiments like the one in Fig. 5*B*: *S*, 2.5 ± 0.372 A.U.; *XL*, 0.588 ± 0.053 A.U., $p < 0.001$) indicating that the non-AUG of TRPV6-XL is less efficient in translation initiation than the AUG in TRPV6-S. However, Ca^{2+} entry monitored by Fura-2 measurements was similar in cells expressing TRPV6-S and TRPV6-XL, respectively (Fig. 5*D*).

For whole cell patch clamp experiments, 10 mM BAPTA in the patch pipette buffering intracellular Ca^{2+} to 0 and 10 mM Ca^{2+} in the external solution were used to activate and measure TRPV6, respectively. To show only net TRPV6-mediated currents, basic currents at break-in were subtracted (*inset* in Fig. 5*F*). Within a few seconds after establishing whole-cell mode, an inward current with typical Ca^{2+}-selective current-voltage relationship (16) appeared in all cells expressing whichever variant of TRPV6 (Fig. 5, *E* and *F*). The shape of the IVs was the same for all three variants (Fig. 5*F*). Corresponding to Fura-2 measurements (Fig. 5*D*), the amplitude of the inward current in TRPV6-S- and TRPV6-XL-expressing cells was almost identical, whereas TRPV6-L-expressing cells revealed significantly higher amplitudes. The (small) TRPV6 channels are known to reveal prominent monovalent cation permeability in the absence of external divalent cations (4, 22, 23). Application of divalent-free (*DVF*) saline induced a huge increase of the inward current in all three variants of TRPV6 (Fig. 5, *G* and *H*). Other than the amplitude, which was slightly larger in TRPV6-L-expressing cells, probably due to the higher initial current (see also Fig. 5*E*), the kinetics of current development (Fig. 5*G*) and IVs (Fig. 5*H*) in divalent-free solution did not differ for TRPV6-S, TRPV6-L, and TRPV6-XL channels.

Changing the holding potential (V_h) after TRPV6 current development from 0 to +60 mV resulted in an increase of the TRPV6 currents, which was very similar for all three variants (Fig. 5, *I* (current-voltage relationships) and *K*). Changing the holding potential from 0 to −60 mV resulted in a total inactivation of the currents within 60 s (Fig. 5, *J* (current-voltage relationships *inset*) and *K*, on top of the voltage axis). Time scale and magnitude of the hyperpolarization-induced inactivation was apparently the same in cells expressing TRPV6-S, -L, and -XL cDNAs. To further compare the kinetics, *i.e.* fast and slow components, of the hyperpolarization-induced voltage- and Ca^{2+}-dependent inactivation (22, 24) of the three TRPV6 variants, a 400-ms and a 10-s voltage step to −100 mV was applied after complete TRPV6 development, and the inactivating currents were measured at a higher temporal resolution (Figs 5, *L*, *M*, and *N*). Fig. 5*L* shows that in all cells, no matter which TRPV6 channel is present, the 400-ms hyperpolarization to −100 mV resulted in a small transient decrease of the inward current, whereas the 10-s hyperpolarization induced a complete inactivation that was transient after reapplying the initial ramp protocols, too. The normalized higher temporal resolution showed that a fast hyperpolarization-induced inactivation took part within 100 ms and was identical in TRPV6-S, -L, and -XL channels (Fig. 5M). The slow component of the hyperpolarization-induced inactivation, measured during the 10-s voltage step to −100 mV, was also very similar (Fig. 5*N*). Because Ca^{2+} seems to be important for the hyperpolarization-induced inactivation, too, the slightly faster kinetics in TRPV6-L currents might be due to the higher initial Ca^{2+} current amplitude in these cells (see Fig. 5*L*).

Characterization of TRPV6-S and TRPV6-XL Proteins—Data shown in Fig. 5*B* indicate that the amount of TRPV6-S protein is higher by ~80%; apparently, the *in vitro* translation efficiency of the truncated TRPV6-S gives an overestimation of the TRPV6 translation efficiency *in vivo*. The data also show that the amplitudes of Ca^{2+} entry and Ca^{2+} current were identical in TRPV6-S- and TRPV6-XL cDNA-expressing cells. To study

whether a larger fraction of the TRPV6-XL protein is associated with the plasma membrane, confocal fluorescence microscopy was performed. The red fluorescent protein mCherry (14) fused to the transferrin receptor membrane anchor (15) (CherryPicker®) was used as a plasma membrane marker. After co-transfecting HEK 293 cells with the CherryPicker cDNA and with the TRPV6-XL or TRPV6-S cDNAs, respectively, fused to the GFP cDNA, the distribution of TRPV6-XL and TRPV6-S perpendicular to the cell membrane was studied in fluorescence images (Fig. 6*A* and supplemental Fig. 1) using dedicated software (see "Experimental Procedures"). Weighted means and 95% confidence intervals were calculated for the normalized intensities of each protein (TRPV6-XL, 48 membrane segments from 32 cells; TRPV6-S, 38 segments from 22 cells) using the number of scan lines in each membrane sample as a weight. The resulting curves are shown in Fig. 6*Aa*. As can be seen, CherryPicker and tmem 16a, the Ca^{2+}-activated chloride channel protein, fused to GFP, which was expressed as an independent control (95 segments from 32 cells), both, peak at the cell membrane, whereas TRPV6-XL and TRPV6-S appear not to be

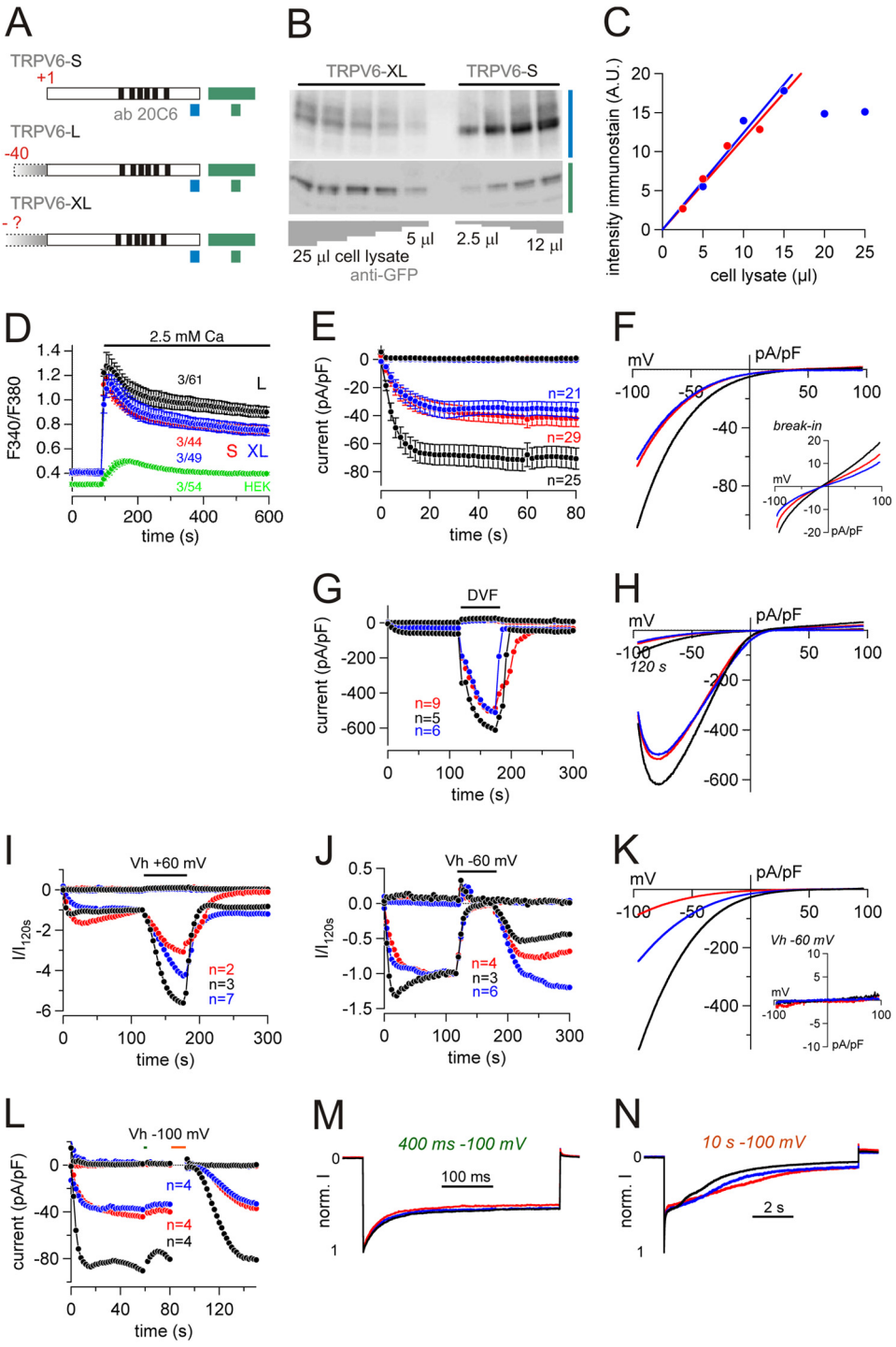

strongly associated with the membrane. As judged from the overlap of the 95% confidence intervals of their fluorescence distributions, the distribution of the two TRP channels between the cytosol and cell membrane appears to be almost identical. Apparently, only a minor and different fraction of the two TRPV6 variants was associated with the membrane, which escaped confocal analysis. Similar results have been obtained for the overexpressed *TRPV5*; the amount of TRPV5 protein routed to the plasma membrane was too small to be detectable by confocal laser scanning microscopy but sufficient for current recordings (25). Most probably, only those cells survive after heterologous overexpression of the TRPV6 or TRPV5 cDNAs, which allow very minor amounts of channel proteins to be targeted to the plasma membrane to prevent deleterious Ca^{2+} entry, and these amounts are not adequate to be identified by fluorescence microscopy.

Surface biotinylation allows the identification of extracellular exposed proteins, and we used this method to assess the amount of TRPV6 protein associated with the plasma membrane (Fig. 6*B*). According to the intensity of the immunostain of the biotinylated TRPV6 proteins the TRPV6-XL is more efficiently associated with the plasma membrane by 2.3-fold compared with TRPV6-S (TRPV6-XL, 2.55 ± 0.56 A.U.; TRPV6-S, 1.14 ± 0.24 A.U.; $n = 11$ experiments, $p < 0.05$). Degradation of both variants assessed by cycloheximide chase experiments (Fig. 6*C*) was not different. Independent of the TRPV6 variant, TRPV6-GFP-fusion proteins were less stable (Fig. 6*Ca*, 27.95 ± 2.18% detectable 24 h after treatment) than the non-fused proteins (Fig. 6*Cb*, 63.83 ± 5.59%; $n = 4$, $p < 0.01$). The extended N terminus (Met^{-40} to Arg^{+26}) is sufficient to pull down full-length TRPV6-XL (Fig. 6*D*), indicating that it is an additional scaffold for channel assembly. In summary, a larger fraction of the TRPV6-XL protein is associated with the plasma membrane, which may compensate for the lower translation of the TRPV6-XL cDNA.

DISCUSSION

In this study we used an antibody-based affinity purification scheme to enrich the endogenous TRPV6 protein from human placenta and the human breast cancer cell line T47D. In SDS-PAGE, the human TRPV6 protein was detectable at a slightly higher apparent molecular weight than the protein expressed from the predicted coding sequence (Fig. 1, *A* and *B*). By applying immunohistochemistry (Fig. 2), site-directed mutagenesis (Fig. 3), *in vitro* translation using a cell-free system (Fig. 3), and mass spectrometry (Fig. 4), we show that the endogenous protein contains an extended N terminus. Translation starts exclusively at a non-AUG codon, at ACG encoding a Thr, but was decoded by Met^{-40} amino acid residues upstream of the canonical and annotated initiation Met. The identified Met^{-40} is the exclusive start of the endogenous human TRPV6 protein and most probably of the mouse TRPV6 protein. The results allow the conclusion that it is the elongated TRPV6-XL protein, which is responsible for TRPV6 activity *in vivo*.

The analyses of the genomes of most organisms utilize AUG for initiation of protein translation, and in most cases the annotated sequences are predicted based on the available techniques of open reading frame mapping. Altogether 60–70 mammalian mRNAs have been described (16–18) that utilize or may utilize alternative non-AUG initiation sites within the predicted 5′-UTR for protein translation, like the v-myc myelocytomatosis viral oncogene homolog (26), the cyclin-dependent protein kinase 10 (27), the fibroblast growth factor (28), and the vascular endothelial growth factor (29).

All non-AUG initiation codons differ from the canonical AUG by just one nucleotide, but only for very few of those mRNAs are data available specifying the decoding initiation amino acid. Peptides displayed by the major histocompatibility class I molecules were identified that are not only derived from conventional but also from cryptic translational reading frames, including some without canonical AUG codons (30). By

FIGURE 5. **Functional properties of TRPV6-S, TRPV6-L, and TRPV6-XL.** *A*, shown are the small (*S*), large (*L*), and very large (*XL*) TRPV6 cDNAs (*open bar with six transmembrane domains indicated in black*) as parts of bicistronic IRES-GFP (*green bar*) vectors expressed in HEK 293 cells. Positions of Ab 20C6 (*blue*) and anti-GFP (*green*) are indicated. *B*, shown is an immunoblot. Different amounts (*gray*) of protein lysates from green fluorescent HEK 293 cells expressing TRPV6-XL (*left*) and TRPV6-S (*right*) were separated by gel electrophoresis, blotted, and incubated with Ab 20C6 (*blue*) or the antibody for GFP (*green*, as loading control). *C*, the intensity of the immunostain for GFP (in A.U.) is plotted against 2.5, 5, 8, and 12 μl of lysates from cells transfected with TRPV6-S-IRES-GFP cDNA (*red*) and 5, 10, 15, 20, and 25 μl of lysates from cells transfected with TRPV6-XL-IRES-GFP cDNA (*blue*). The same amount of GFP per μl is detectable after transfection of cells with either cDNA construct. At higher amounts of lysate applied (20 and 25 μl), the intensity saturates. The estimation of the amount of expressed TRPV6-S and TRPV6-XL is based on the amount of GFP calculated only for the linear part of this plot. A representative experiment from three experiments is shown. *D*, cells from the same transfection as in *B* were loaded with Fura-2-AM and kept in nominally Ca^{2+}-free bath solution. Ca^{2+} influx was challenged by adding 2.5 mM Ca^{2+} to the bath solution, and cytosolic Ca^{2+} concentration, represented by the Fura-2 fluorescence ratio (F_{340}/F_{380}), was measured *versus* time. TRPV6-S (*red*), TRPV6-L (*black*), TRPV6-XL (*blue*), and non-transfected HEK 293 cells (*green*) are shown. Data represent the means ± S.E. with *x* averaged experiments including *n* measured cells (*x*/*n*). *E–N*, reducing intracellular Ca^{2+} induces Ca^{2+} inward currents in TRPV6-expressing HEK 293 cells. *E*, shown is net development of low intracellular Ca^{2+}-induced inward and outward currents at −80 and +80 mV, respectively, plotted *versus* time. *F*, shown are the corresponding current-voltage relationships (IVs) at maximum currents in *E* and the *inset* directly after establishing whole cell configuration (basic current at break-in). Data in *E* represent the means ± S.E. with *n* averaged experiments. *G* and *H*, in the absence of extracellular divalent cations, the S, L, and XL variants of TRPV6 become permeable to monovalent cations. *G*, shown is net development of low intracellular Ca^{2+}-induced inward and outward currents at −80 and +80 mV, respectively, plotted *versus* time. At the indicated time (*black bar*) divalent-free (*DVF*) saline was transiently applied, leading to a huge increase of the inward current. *H*, corresponding current-voltage relationships right before application of divalent-free saline (120 s) and at maximum currents during divalent-free application (180 s) in *G*. *I—N*, shown is voltage dependence of the small, large, and very large variant of TRPV6. *I* and *J*, shown is net development of low intracellular Ca^{2+}-induced inward and outward currents at −80 and +80 mV, respectively, plotted *versus* time and normalized to the current size at −80 mV at 120 s (I/I_{120s}). At the indicated times (*black bar*) the holding potential (V_h) was transiently changed from 0 to +60 mV (*I*) and −60 mV (*J*), leading to a significant increase and a complete block of the inward current, respectively. *K*, shown are the corresponding IVs of the maximal current at V_h 60 mV and minimal current at V_h −60 mV (inset). *L*, shown is net development of low intracellular Ca^{2+}-induced inward and outward currents at −80 and +80 mV, respectively, plotted *versus* time. At the indicated times a 400-ms (*green*) and a 10-s voltage step (*orange*) to −100 mV were applied. *M* and *N*, normalized changes of the inward current at the 400 ms (*M*) and 10 s (*N*) voltage step to −100 mV show the "fast" and "slow" hyperpolarization-dependent inactivation, respectively. Data in *F–N* represent the means with *n* averaged experiments (for current-voltage relationships, see the corresponding traces) but without S.E. for a better differentiation of the traces. *pA/pF*, picoamperes/picofarads.

comparing *e.g.* reverse phase-HPLC elution times of endogenous and synthetic peptides, the CUG codon was shown to be decoded as leucine (31), and it was concluded that CUG/Leu-tRNA initiation was independent of the canonical tRNA (AUG/Met-$tRNA_i^{Met}$) pathway (30). Initiation of the mRNA for the human phosphoribosyl pyrophosphate synthase III (PRPS1L1) occurs at an ACG codon (for threonine), but from *in vitro* translation of the mRNA it seemed that the protein probably starts with Met at the N-terminal position corresponding to the ACG (20).

The experimentally determined optimal context for efficient initiation at vertebrate translational start sites (GCCACCAUGG) closely matches the "consensus" sequence (GCCGCCA/GCCAUGG) of their mRNAs revealed by statistical analyses (12, 32). Our data demonstrate that translation of the TRPV6 mRNA initiates at the ACG codon (positions −120 to −118) within the 5′-UTR and that this codon is decoded by Met. The identified TRPV6 initiation site ACG differs from AUG by just one nucleotide, and the anticodon of an initiator tRNA appears to be compensated for by interactions with nearby nucleotides, in particular the G at position −3 (position −123 of the TRPV6 sequence) and a G at position +4 (position −117). The non-canonical ACG triplet is placed in a good Kozak context (gagACGg) in the 5′-UTR, whereas the assumed initiation AUG (cccAUGg) is not. This indicates that the upstream ACG context offers an enlarged initiation capacity. Moreover, palindromes with the potential forming stem-loop structures exist immediately downstream of the ACG

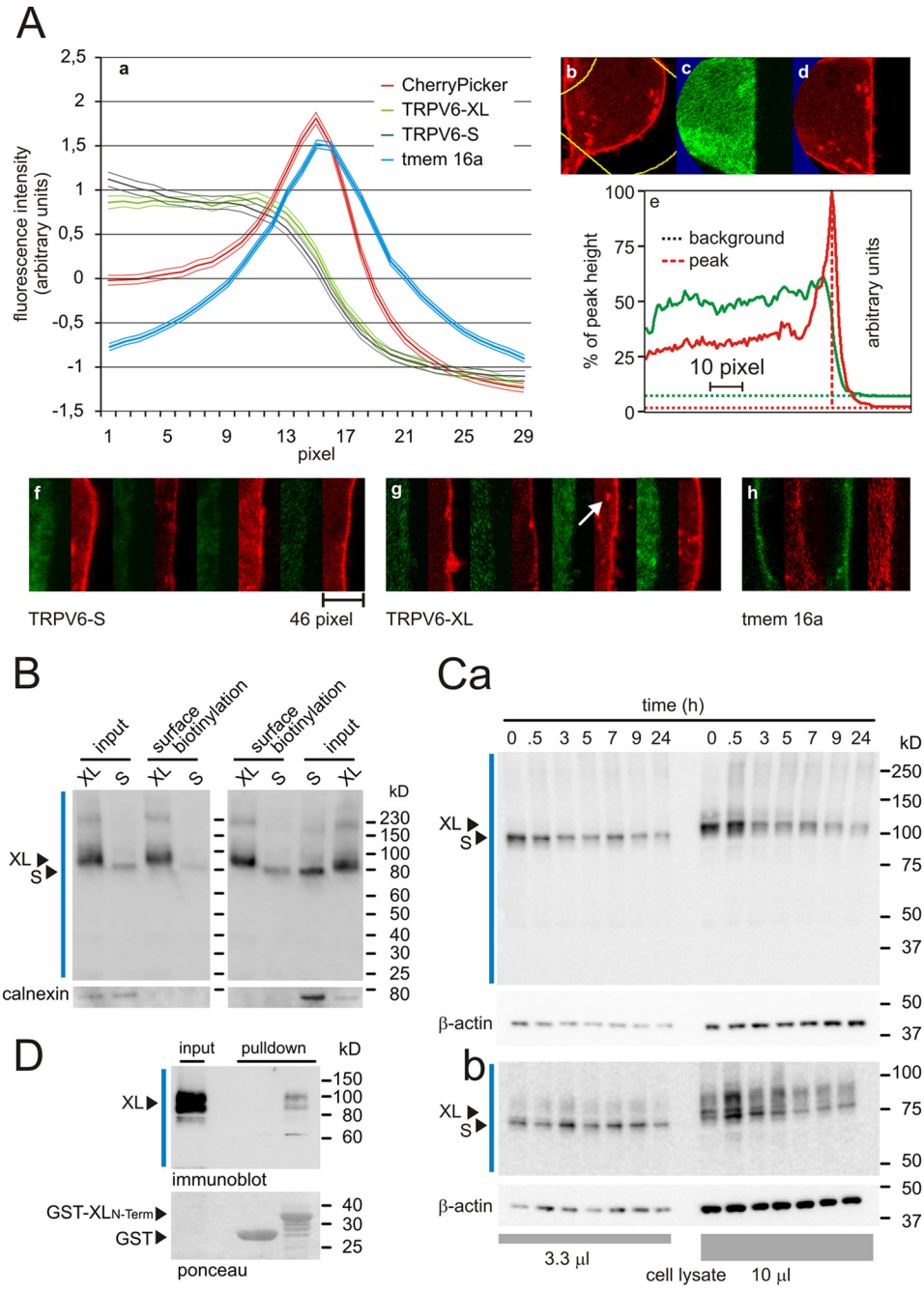

A

```
                                                                                                                +1
human       SALQRAPPPPGKALLPRQGGQSPQRTCMHTHHLTTHCMHTHTPQPHTVHTRTPHNPHTACTHTHLQAACCIHKSYRR*TQSPSPK*TPSLAQLLSS*TCFFRHISIICQCLQGEDMGGF.
gibbon      ----------------------TTHCMQTHHLKTTHCMHTHTPQPHTVHTHTPHNPHTACTHTHPQAAWCVHKSYRK*TQSPSPKQTPSLAQLLSS*TCFFHHISIIC*CLQGEDMGGF.
horse       ------------------------------------------------------------------------------------AAEP-----------*TCSFYHILITCQYLKGEDMGAP.
rabbit      ------------------------------------------------------------------------------PQPALPPP--QLLLS*TCSS*HIPTTCQCLQGADMGAC.
mouse       ------------------------------------------------------------------------P----LSS-----------*TGSFHEI*TSCKYVQ-EDMGAK.
rat         ------------------------------------------------------------GTYSHLTATHCVGNKLPGDIYLSSP*QT*T-PQLLSP*TDSFHEIRISGWYLH-EDMGVK.
```

B

```
ANK              .G.TPLHLAA..--------GVVLLLGA-----------------------
V6-XL      -10   PKEPALHPMGLSLPK---EKGLILCLWSKFCRWFQRRESWAQSRDEQNLLQ
V6 ank1     44   IWESPLLLAAKDND----VQALNKLLKYEDCKVHQRGA-------------
V6 ank2     78   MGETALHIAALYDN----LEAAMVLMEAAPELVFEPMTSELY---------
V6 ank3    116   EGQTALHIAVVNQN----MNLVRALL-ARRASVSARATGTAFRRSPRNLIY
V6 ank4    162   FGEHPLSFAACVNS----EEIVRLLIEHGADIRAQDS--------------
V6 ank5    195   LGNTVLHILILQPNKTFACQMYNLLLSYDRHGDHLQPLDLVPNH-------
V6 ank6    238   QGLTPFKLAGVEGN----TVMFQHLMQKRKHT--------------------
```

FIGURE 7. *A*, shown is MUSCLE multiple sequence alignment of the translated 5′-UTR of TRPV5 as available from the Ensembl genome browser. Identical aa residues are *shaded*; annotated N termini with the first methionine as +1 are in *red*; * (*yellow*), stop codon in frame; -, gap. B, shown is alignment of the ankyrin repeat domain of TRPV6 including the ankyrin repeat consensus (17), part of the TRPV6-XL sequence, and the six TRPV6 ankyrin repeats. *Shaded*, sequence identity with the consensus; *red*, sequence identity only within the TRPV6 sequences.

codon (Fig. 3*A*, nt −96 to −92 and −87 to −91, nt −41 to −38, and nt −32 to −35), and such structures have been shown to have the capacity of strongly enhancing the use of both AUG and non-AUG initiators (33–35).

As shown in Fig. 1, *D* and *E*, and 3*E*, the first AUG codon of the TRPV6 mRNA is not used for the initiation of translation, and translation is exclusively initiated at the ACG codon 120-bp upstream of the first AUG codon. Downstream of the ACG codon, an inverted repeat can be identified. This may result in a hairpin folding and, therefore, could render initiation of the translation from the first AUG codon. According to the scanning model of translation in eukaryotic cells described in detail by Kozak (36, 37), the ribosomes attach near the cap structure of the mRNA and scan downstream to the first AUG codon and, if placed in an appropriate context, initiate translation. However if the first AUG of a given mRNA is deleted or mutated, the ribosomes can initiate translation from a downstream localized AUG codon. If we mutate the initiation ACG codon of the TRPV6 mRNA in a way that two bases differ from the classical AUG codon, the initiation of translation dramatically drops. This effect was seen in overexpressing cells and in the cell-free *in vitro* translation system (Fig. 3*C* and *E*). However, we suppose that the hairpin structure of the TRPV6 mRNA inhibits downstream scanning of the ribosomes, and therefore, the initiation of translation from another AUG codon is blocked.

TRPV5 is the closest relative to TRPV6 sharing 74% amino acid sequence identity. However, the 5′-UTRs of *TRPV5* (Fig. 7*A*), like the 5′-UTRs of the *TRPV1*, *TRPV2*, *TRPV3* and *TRPV4* genes, contain several stop codons immediately 5′ of their respective initiation AUG codons. Thus these *TRPV* genes might be translated from the first AUG of their mRNA.

TRPV6 proteins are responsible for Ca^{2+} uptake in various tissues including the epididymis and the prostate (4–6); in placental trophoblasts, it may contribute to the transfer of Ca^{2+} from mother to fetus (38). We found in HEK cells the channel properties of TRPV6-XL to be very similar to those of TRPV6-S (Fig. 5, *E–K*). In heterologous expression experiments, the initiation of translation at the AUG site of the S version is ~5-fold as efficient as initiation at the non-AUG of the XL-version (Fig. 5*B*), which is used *in vivo*. Considering that the Ca^{2+} uptake by cells has to be tightly regulated to prevent deleterious Ca^{2+}

FIGURE 6. *A*, shown is distribution of TRPV6-XL and TRPV6-S fused to GFP perpendicular to the cell membrane. *Aa*, shown is cumulative distribution of TRPV6-XL (*green*; 48 membrane segments from 32 cells), TRPV6-S (*dark magenta*; 38 segments from 22 cells), and tmem 16a (*cyan*; 95 segments from 32 cells) perpendicular to the membrane (means ± 95% confidence intervals). tmem 16a or anoctamin 1 is a Ca^{2+}-activated chloride channel protein used here as an independent control. The peaks of the CherryPicker fluorescence (*red*) of all membrane segments were taken as a marker for the cell membrane and were used to align individual samples (red fluorescence in *A*, *b*, *d*, *f*, *g*, and *h*). All curves are weighted means of the z- and least squares-transformed fluorescence intensities with the number of scan lines in each sample as a weight. *Ab*, using dedicated software, starting as well as end points of appropriate membrane samples were defined, and the image was rotated so that the selected membrane segment was angled vertically (*A*, *f*, *g*, and *h*). *A*, *c* and *d*, shown are the vertically aligned membrane segments were linearized by cross-correlation of individual scan lines with the center scan line of the membrane segment. To minimize the influence of hot spots of fluorescence on the linearization (*arrow mark* in *Ag*), the membrane was traced manually with a digitizing tablet, the manual trace was smoothed by a moving average filter, and a region of interest was defined to the left and right of the cell membrane, which entered the cross correlation algorithm (39). After linearization, fluorescence intensities were added column-wise and displayed as a curve. The peak of the red fluorescence as well as the background value for each fluorescence channel was determined automatically by the software with manual correction if required. A, *b*, *c*, *d*, and *e*, samples were derived from one membrane specimen. A, *f* and *g*, four typical samples each of membrane segments from cells transfected with cDNAs for TRPV6-S-GFP or TRPV6-XL-GFP, respectively (*green fluorescence*) are shown. Each sample has a height of 126 scan lines (21). Two membrane samples from cells transfected with tmem 16a-GFP cDNA (*green fluorescence*) served as the control. *B*, immunoblots of surface-expressed TRPV6-XL (*XL*) and TRPV6-S (*S*) cDNAs were detected by Ab 20C6 (*blue*). The endoplasmic reticulum protein calnexin was used as the control. *C*, shown is a comparison of protein stability of TRPV6-S and TRPV6-XL at the indicated time points after cycloheximide treatment. To allow adequate densitometric analysis of the intensity of the antibody stain, only one-third of the amount of protein lysate from TRPV6-S-transfected cells was applied per lane compared with protein lysate from TRPV6-XL-transfected cells. Shown is an immunoblot with Ab 26B3 for TRPV6; β-actin was used as an independent control. TRPV6 proteins were fused to GFP (*Ca*) and non-fused TRPV6 (*Cb*). *D*, HEK 293 cell lysate of TRPV6-XL (*input XL*) was incubated with either the GST or GST-TRPV6-XL N terminus bound to glutathione-agarose. Bound proteins were separated on SDS-PAGE and blotted, and the membrane was stained with Ponceau red (*lower panel*, input control of GST and GST fusion protein) and then incubated with antibody 429 (*upper panel*, immunoblot), ($n = 2$).

overload, the potential advantage of the initiation at the ACG site *in vivo* could provide a mechanism for modulating Ca^{2+} entry at the level of synthesis of channel subunits.

The additional 40-aa sequence shows no similarity to any known protein sequence, and it does not affect the stability of the protein. Nine out of the 40 amino acid residues are Pro, and they might well constitute motifs involved in protein-protein interaction mediated by SH3 domains. The elongated N terminus may enhance plasma membrane localization because (i) the fraction of TRPV6-XL being biotinylated at the cell surface is larger than the corresponding fraction of TRPV6-S, and (ii) the current amplitude and the amplitude of Fura-2-measured Ca^{2+} entry is similar for both channel types although the XL version is expressed to a lesser extent. Homo- and tetramerization of TRPV channels may depend on residues in all three regions of the proteins, the N- and C-terminal cytosolic domains and the transmembrane domain (39), but two of the six ankyrin repeats (4, 40) of the TRPV6 protein repeats 3 and 5 (41) have been indicated in channel assembly. Part of the extended TRPV6 N terminus shows some similarity to the TRPV6 ankyrin repeats (Fig. 7*B*) and may contribute to multimerization, and accordingly, the pulldown experiments (Fig. 6*D*) show that the N terminus of TRPV6-XL binds to the TRPV6-XL full-length protein.

Initiation of translation from a non-AUG codon may be greatly underestimated and underreported. In addition it is imaginable that translation initiation at such codons may occur only under specific circumstances that are not typically encountered in empirical systems in the laboratory.

The necessity that TRPV6 proteins require an elongated N terminus starting with a non-AUG codon is not obvious. But it is striking that the elongated TRPV6-XL protein is more effective than the artificially expressed short variant; for a comparable current amplitude, TRPV6-expressing cells have to synthesize ~5-fold less TRPV6-XL than TRPV6-S. This feature enables TRPV6-expressing cells to regulate dynamically channel expression and calcium uptake.

Proteins as diverse as S100A10-annexin 2, the PDZ protein Na^+/H^+ exchanger regulatory factor 4 (NHERF4), and Rab11a (42) have been suggested to interact with TRPV6 *in vivo* to regulate the trafficking, the anchoring, and the activity of TRPV6 proteins at the plasma membrane. The binding sites for these proteins, like one for Ca^{2+}-calmodulin (24), have been mapped exclusively to the cytosolic C terminus of TRPV6. In summary, the elongated N terminus may not only stabilize and increase the fraction of plasma membrane-localized multimeric channels but also represents a binding domain for homomeric interaction and presumably for yet to be identified interacting proteins and regulatory molecules.

Acknowledgments—We thank Karin Wolske, Heidi Löhr, and Christine Wesely for expert technical assistance and Dr. Peter Lipp for use of and help with the confocal microscope.

REFERENCES

1. Wu, L. J., Sweet, T. B., and Clapham, D. E. (2010) International Union of Basic and Clinical Pharmacology. LXXVI. Current progress in the mammalian TRP ion channel family. *Pharmacol. Rev.* **62,** 381–404
2. Peng, J. B., Chen, X. Z., Berger, U. V., Vassilev, P. M., Tsukaguchi, H., Brown, E. M., and Hediger, M. A. (1999) Molecular cloning and characterization of a channel-like transporter mediating intestinal calcium absorption. *J. Biol. Chem.* **274,** 22739–22746
3. Peng, J. B., Chen, X. Z., Berger, U. V., Weremowicz, S., Morton, C. C., Vassilev, P. M., Brown, E. M., and Hediger, M. A. (2000) Human calcium transport protein CaT1. *Biochem. Biophys. Res. Commun.* **278,** 326–332
4. Wissenbach, U., Niemeyer, B. A., Fixemer, T., Schneidewind, A., Trost, C., Cavalie, A., Reus, K., Meese, E., Bonkhoff, H., and Flockerzi, V. (2001) Expression of CaT-like, a novel calcium-selective channel, correlates with the malignancy of prostate cancer. *J. Biol. Chem.* **276,** 19461–19468
5. Weissgerber, P., Kriebs, U., Tsvilovskyy, V., Olausson, J., Kretz, O., Stoerger, C., Mannebach, S., Wissenbach, U., Vennekens, R., Middendorff, R., Flockerzi, V., and Freichel, M. (2012) Excision of Trpv6 gene leads to severe defects in epididymal Ca^{2+} absorption and male fertility much like single D541A pore mutation. *J. Biol. Chem.* **287,** 17930–17941
6. Weissgerber, P., Kriebs, U., Tsvilovskyy, V., Olausson, J., Kretz, O., Stoerger, C., Vennekens, R., Wissenbach, U., Middendorff, R., Flockerzi, V., and Freichel, M. (2011) Male fertility depends on Ca^{2+} absorption by TRPV6 in epididymal epithelia. *Sci. Signal.* **4,** ra27
7. Hirnet, D., Olausson, J., Fecher-Trost, C., Bödding, M., Nastainczyk, W., Wissenbach, U., Flockerzi, V., and Freichel, M. (2003) The TRPV6 gene, cDNA, and protein. *Cell Calcium* **33,** 509–518
8. Stumpf, T., Zhang, Q., Hirnet, D., Lewandrowski, U., Sickmann, A., Wissenbach, U., Dörr, J., Lohr, C., Deitmer, J. W., and Fecher-Trost, C. (2008) The human TRPV6 channel protein is associated with cyclophilin B in human placenta. *J. Biol. Chem.* **283,** 18086–18098
9. Bolanz, K. A., Hediger, M. A., and Landowski, C. P. (2008) The role of TRPV6 in breast carcinogenesis. *Mol. Cancer Ther.* **7,** 271–279
10. Simkin, D., Cavanaugh, E. J., and Kim, D. (2008) Control of the single channel conductance of K2P10.1 (TREK-2) by the amino terminus. Role of alternative translation initiation. *J. Physiol.* **586,** 5651–5663
11. Thomas, D., Plant, L. D., Wilkens, C. M., McCrossan, Z. A., and Goldstein, S. A. (2008) Alternative translation initiation in rat brain yields K2P2.1 potassium channels permeable to sodium. *Neuron* **58,** 859–870
12. Kozak, M. (1987) At least six nucleotides preceding the AUG initiator codon enhance translation in mammalian cells. *J. Mol. Biol.* **196,** 947–950
13. Candiano, G., Bruschi, M., Musante, L., Santucci, L., Ghiggeri, G. M., Carnemolla, B., Orecchia, P., Zardi, L., and Righetti, P. G. (2004) Blue silver. A very sensitive colloidal Coomassie G-250 staining for proteome analysis. *Electrophoresis* **25,** 1327–1333
14. Shaner, N. C., Campbell, R. E., Steinbach, P. A., Giepmans, B. N., Palmer, A. E., and Tsien, R. Y. (2004) Improved monomeric red, orange, and yellow fluorescent proteins derived from *Discosoma* sp. red fluorescent protein. *Nat. Biotechnol.* **22,** 1567–1572
15. Winnard, P. T., Jr., Kluth, J. B., Kato, Y., Artemov, D., and Raman, V. (2007) Development of novel chimeric transmembrane proteins for multimodality imaging of cancer cells. *Cancer Biol. Ther.* **6,** 1889–1899
16. Ivanov, I. P., Firth, A. E., Michel, A. M., Atkins, J. F., and Baranov, P. V. (2011) Identification of evolutionarily conserved non-AUG-initiated N-terminal extensions in human coding sequences. *Nucleic Acids Res.* **39,** 4220–4234
17. Tikole, S., and Sankararamakrishnan, R. (2006) A survey of mRNA sequences with a non-AUG start codon in RefSeq database. *J. Biomol. Struct. Dyn.* **24,** 33–42
18. Wegrzyn, J. L., Drudge, T. M., Valafar, F., and Hook, V. (2008) Bioinformatic analyses of mammalian 5′-UTR sequence properties of mRNAs predicts alternative translation initiation sites. *BMC Bioinformatics* **9,** 232
19. Peabody, D. S. (1987) Translation initiation at an ACG triplet in mammalian cells. *J. Biol. Chem.* **262,** 11847–11851
20. Taira, M., Iizasa, T., Shimada, H., Kudoh, J., Shimizu, N., and Tatibana, M. (1990) A human testis-specific mRNA for phosphoribosylpyrophosphate synthetase that initiates from a non-AUG codon. *J. Biol. Chem.* **265,** 16491–16497
21. Old, W. M., Meyer-Arendt, K., Aveline-Wolf, L., Pierce, K. G., Mendoza, A., Sevinsky, J. R., Resing, K. A., and Ahn, N. G. (2005) Comparison of label-free methods for quantifying human proteins by shotgun proteomics. *Mol. Cell Proteomics* **4,** 1487–1502

22. Voets, T., Prenen, J., Fleig, A., Vennekens, R., Watanabe, H., Hoenderop, J. G., Bindels, R. J., Droogmans, G., Penner, R., and Nilius, B. (2001) CaT1 and the calcium release-activated calcium channel manifest distinct pore properties. *J. Biol. Chem.* **276,** 47767–47770
23. Yue, L., Peng, J. B., Hediger, M. A., and Clapham, D. E. (2001) CaT1 manifests the pore properties of the calcium release-activated calcium channel. *Nature* **410,** 705–709
24. Niemeyer, B. A., Bergs, C., Wissenbach, U., Flockerzi, V., and Trost, C. (2001) Competitive regulation of CaT-like-mediated Ca^{2+} entry by protein kinase C and calmodulin. *Proc. Natl. Acad. Sci. U.S.A.* **98,** 3600–3605
25. den Dekker, E., Schoeber, J., Topala, C. N., van de Graaf, S. F., Hoenderop, J. G., and Bindels, R. J. (2005) Characterization of a Madin-Darby canine kidney cell line stably expressing TRPV5. *Pflugers Arch.* **450,** 236–244
26. Hann, S. R., King, M. W., Bentley, D. L., Anderson, C. W., and Eisenman, R. N. (1988) A non-AUG translational initiation in c-myc exon 1 generates an N-terminally distinct protein whose synthesis is disrupted in Burkitt's lymphomas. *Cell* **52,** 185–195
27. Graña, X., Claudio, P. P., De Luca, A., Sang, N., and Giordano, A. (1994) PISSLRE, a human novel CDC2-related protein kinase. *Oncogene* **9,** 2097–2103
28. Arnaud, E., Touriol, C., Boutonnet, C., Gensac, M. C., Vagner, S., Prats, H., and Prats, A. C. (1999) A new 34-kilodalton isoform of human fibroblast growth factor 2 is cap-dependently synthesized by using a non-AUG start codon and behaves as a survival factor. *Mol. Cell. Biol.* **19,** 505–514
29. Tee, M. K., and Jaffe, R. B. (2001) A precursor form of vascular endothelial growth factor arises by initiation from an upstream in-frame CUG codon. *Biochem. J.* **359,** 219–226
30. Starck, S. R., Jiang, V., Pavon-Eternod, M., Prasad, S., McCarthy, B., Pan, T., and Shastri, N. (2012) Leucine-tRNA initiates at CUG start codons for protein synthesis and presentation by MHC class I. *Science* **336,** 1719–1723
31. Schwab, S. R., Shugart, J. A., Horng, T., Malarkannan, S., and Shastri, N. (2004) Unanticipated antigens. Translation initiation at CUG with leucine. *PLoS Biol.* **2,** e366
32. Kozak, M. (1994) Determinants of translational fidelity and efficiency in vertebrate mRNAs. *Biochimie* **76,** 815–821
33. Kozak, M. (1991) An analysis of vertebrate mRNA sequences. Intimations of translational control. *J. Cell Biol.* **115,** 887–903
34. Kozak, M. (1991) Structural features in eukaryotic mRNAs that modulate the initiation of translation. *J. Biol. Chem.* **266,** 19867–19870
35. Xiao, J. H., Davidson, I., Matthes, H., Garnier, J. M., and Chambon, P. (1991) Cloning, expression, and transcriptional properties of the human enhancer factor TEF-1. *Cell* **65,** 551–568
36. Kozak, M. (1978) How do eucaryotic ribosomes select initiation regions in messenger RNA? *Cell* **15,** 1109–1123
37. Kozak, M. (1989) The scanning model for translation. An update. *J. Cell Biol.* **108,** 229–241
38. Suzuki, Y., Kovacs, C. S., Takanaga, H., Peng, J. B., Landowski, C. P., and Hediger, M. A. (2008) Calcium channel TRPV6 is involved in murine maternal-fetal calcium transport. *J. Bone Miner. Res.* **23,** 1249–1256
39. Hellwig, N., Albrecht, N., Harteneck, C., Schultz, G., and Schaefer, M. (2005) Homo- and heteromeric assembly of TRPV channel subunits. *J. Cell Sci.* **118,** 917–928
40. Phelps, C. B., Huang, R. J., Lishko, P. V., Wang, R. R., and Gaudet, R. (2008) Structural analyses of the ankyrin repeat domain of TRPV6 and related TRPV ion channels. *Biochemistry* **47,** 2476–2484
41. Erler, I., Hirnet, D., Wissenbach, U., Flockerzi, V., and Niemeyer, B. A. (2004) Ca^{2+}-selective transient receptor potential V channel architecture and function require a specific ankyrin repeat. *J. Biol. Chem.* **279,** 34456–34463
42. van de Graaf, S. F., Hoenderop, J. G., and Bindels, R. J. (2006) Regulation of TRPV5 and TRPV6 by associated proteins. *Am. J. Physiol. Renal Physiol.* **290,** F1295–F1302